

Shape and Motion of Vortex Cores in $\text{Bi}_2\text{Sr}_2\text{CaCu}_2\text{O}_{8+\delta}$

B.W. Hoogenboom*, M. Kugler, B. Revaz†, I. Maggio-Aprile, and Ø. Fischer
DPMC, Université de Genève, 24 Quai Ernest-Ansermet, 1211 Genève 4, Switzerland

Ch. Renner

NEC Research Institute, 4 Independence Way, Princeton, New Jersey 08540, USA
(June 1, 2018)

We present a detailed study on the behaviour of vortex cores in $\text{Bi}_2\text{Sr}_2\text{CaCu}_2\text{O}_{8+\delta}$ using scanning tunneling spectroscopy. The very irregular distribution and shape of the vortex cores imply a strong pinning of the vortices by defects and inhomogeneities. The observed vortex cores seem to consist of two or more randomly distributed smaller elements. Even more striking is the observation of vortex motion where the vortex cores are divided between two positions before totally moving from one position to the other. Both effects can be explained by quantum tunneling of vortices between different pinning centers.

PACS numbers: 74.50.+r, 74.60.Ec, 74.60.Ge, 74.72.Hs

I. INTRODUCTION

The study of the vortex phases in high temperature superconductors (HTS's) has lead to both theoretical predictions of several novel effects and experiments accompanied by challenging interpretations. The reasons are multiple. First, the unconventional symmetry of the order parameter — most likely $d_{x^2-y^2}$ — leads to the presence of low-lying quasiparticle excitations near the gap nodes, which in turn has inspired the predictions of a nonlinear Meissner effect¹, of a \sqrt{H} dependence of the density of states at the Fermi level near the vortex cores $(N(0, \mathbf{r}))^2$, and of a four-fold symmetry of the vortices³⁻⁵. However, the experimental evidence for the first two effects is still controversial⁶⁻⁹, and scanning tunneling spectroscopy (STS) measurements on vortex cores have not shown any clear signature of a \sqrt{H} dependence of $N(0, \mathbf{r})$ ^{10,11}. Concerning the four-fold symmetry, a tendency of square vortices was found in previous measurements¹¹, but inhomogeneities make it difficult to be decisive about it. Interestingly, a four-fold symmetry has been observed around single atom zinc impurities in $\text{Bi}_2\text{Sr}_2\text{CaCu}_2\text{O}_{8+\delta}$ (BSCCO), which are of a smaller size than the vortex cores¹².

A second reason is related to the interaction of vortices with pinning centers, responsible for the rich vortex phase diagram of the HTS's¹³. The pinning of vortices is mainly due to local fluctuations of the oxygen concentration¹⁴⁻¹⁷, and facilitated by their highly 2D "pancake" character. In BSCCO the areal density of oxygen vacancies per Cu-O double layer is in fact surprisingly large: 10^{17} m^{-2} ¹⁶, corresponding to an average distance between the oxygen vacancies of the order of 10 Å. This vortex pinning results for BSCCO in the absence of any regular flux line lattice at high fields, as demonstrated by both neutron diffraction¹⁸ and STS¹¹ experiments. Moreover, since the distance between the oxygen vacancies is of the order of the vortex core size,

one may expect that not only the vortex distribution, but also the vortex core shape will be dominated by pinning effects, and *not* by intrinsic symmetries like that of the order parameter. A detailed understanding of the interaction of vortices with pinning centers will thus be of importance to explain the lack of correspondence between theoretical predictions about the vortex shape and STS measurements.

Third, and again as a consequence of the anisotropy of the order parameter, low-energy quasiparticles are not truly localized in the vortex core (contrarily to the situation in *s*-wave superconductors¹⁹⁻²¹). For pure *d*-wave superconductors these quasiparticles should be able to escape along the nodes of the superconducting gap. Thus in the vortex core spectra one expects a broad zero-bias peak of spatially extended quasiparticle states⁵. However, tunneling spectra of the vortex cores in $\text{YBa}_2\text{Cu}_3\text{O}_{7-\delta}$ (YBCO) showed two clearly separated quasiparticle energy levels, which were interpreted as a signature of localized states¹⁰. In BSCCO two weak peaks have been observed in the some vortex core spectra^{22,23}, suggesting a certain similarity to the behaviour in YBCO. Another important characteristic of HTS's that follows from the STS studies mentioned above, is the extremely small size of the vortex cores in these materials. The large energy separation between the localized quasiparticle states directly implies that the vortex cores in YBCO are of such a size that quantum effects dominate. This is even more true in BSCCO: not only the in-plane dimensions of the vortex cores are smaller than in YBCO and become of the order of the interatomic distances¹¹, but due to the extreme anisotropy of the material also their out-of-plane size is strongly reduced. This highly quantized character of vortices in HTS's is equally demonstrated by the non-vanishing magnetic relaxation rate in the limit of zero temperature, attributed to quantum tunneling of vortices through the energy barriers between subsequent pinning centers¹³.

In this paper we present a detailed STS study of the shape of the vortices in BSCCO. We will show that this shape is influenced by inhomogeneities. The samples presented here, which we characterize as moderately homogeneous, are used to study the behaviour of vortex cores under these conditions. Apart from the vortex core shape, this also includes the evolution in time of the vortices. We will show that both effects can be related to tunneling of vortices between different pinning centers. This is another indication of the possible extreme quantum behaviour of vortex cores in HTS's. A corollary of this paper is that only extremely homogeneous samples will show intrinsic shapes of vortex cores.

II. EXPERIMENTAL DETAILS

The tunneling spectroscopy was carried out using a scanning tunneling microscope (STM) with an Ir tip mounted perpendicularly to the (001) surface of a BSCCO single crystal, grown by the floating zone method. The crystal was oxygen overdoped, with $T_c = 77$ K, and had a superconducting transition width of 1 K (determined by an AC susceptibility measurement). We cleaved *in situ*, at a pressure $< 10^{-8}$ mbar, at room temperature, just before cooling down the STM with the sample. The sharpness of the STM tip was verified by making topographic images with atomic resolution. Tunneling current and sample bias voltage were typically 0.5 nA and 0.5 V, respectively. We performed the measurements at 4.2 K with a low temperature STM described in Ref. 24,25, and those at 2.5 K with a recently constructed ^3He STM²⁶. A magnetic field of 6 T parallel to the *c*-axis of the crystal was applied after having cooled down the sample. The measurements presented here were initiated 3 days after having switched on the field.

The dI/dV spectra measured with the STM correspond to the quasiparticle local density of states (LDOS). In the superconducting state one observes two pronounced coherence peaks, centered around the Fermi level, at energies $\pm\Delta_p$. The gap size Δ_p varied from 30-50 meV. In the vortex cores the spectra are remarkably similar to those of the pseudogap in BSCCO measured above T_c ¹¹, with a total disappearance of the coherence peak at negative bias, a slight increase of the zero bias conductivity, and a decrease and shift to higher energy of the coherence peak at positive bias. To map the vortex cores we define a gray scale using the quotient of the conductivity $\sigma(V_p) = dI/dV(V_p)$ at a negative sample voltage $V_p = -\Delta_p/e$ and the zero bias conductivity $\sigma(0) = dI/dV(0)$. Thus we obtain spectroscopic images, where vortex cores appear as dark spots. Since we measure variations of the LDOS, which occur at a much smaller scale (the coherence length ξ) than the penetration depth λ , we can get vortex images at high fields. A tunneling spectrum is taken on the time scale of seconds,

spectroscopic images typically take several hours (about 12 hours for the images of $100 \times 100 \text{ nm}^2$ presented below). The images therefore necessarily reflect a time-averaged vortex density.

In all large-scale images we have suppressed short length-scale noise by averaging each point over a disk of radius $\sim 20 \text{ \AA}$. When zooming in to study the shape of individual vortices, we strictly used raw data. Further experimental details can be found in previous publications^{11,27,28}.

III. RESULTS

A. Vortex Distribution

In Fig. 1 we show spectroscopic images of the surface of a BSCCO crystal, at different magnetic field strengths. The large dark structure, clearly visible at the right of Figs. 1(b) and (c), corresponds to a degraded region resulting from a large topographic structure, already observed in the topographic image Figs. 1(a). The presence of this structure allows an exact position determination throughout the whole experimental run. As can be seen in Fig. 1, the number of vortices at 6 and at 2 T, in exactly the same region, scales very well with the total number of flux quanta (Φ_0) that one should expect at these field strengths. This clearly proves that the observed dark spots are directly related to vortex cores, and not to inhomogeneities, defects or any form of surface degradation. The large spot in the upper left corner of Fig. 1(c) forms an exception: it appeared after a sudden noise on the tunnel current while we were scanning on that position, showed semiconducting spectra (typical for degraded tunneling conditions) afterwards, and remained even after having set the external field to 0 T. One should however not exclude that a vortex is pinned in this degraded zone. Finally, the size and density of the vortices are fully consistent with previous measurements^{11,23}.

Instead of a well ordered vortex lattice, one observes patches of various sizes and shapes scattered over the surface. This clearly indicates the disordered nature of the vortex phase in BSCCO at high fields, again in consistency with previous STM studies^{11,23} and neutron scattering data¹⁸, and stressing the importance of pinning for the vortex distribution.

B. Vortex Shapes

As a next step we increase the spatial resolution in order to investigate individual vortex cores. Some vortices appear with square shapes, but most vortices in this study have irregular shapes. Closer inspection of the tunneling spectra reveals small zones inside the vortex core that show superconducting behaviour. That is, when scanning through a vortex core one often observes

(slightly suppressed) coherence peaks (Fig. 2(a)), typical for the superconducting state, at some spots *inside* the vortex core. The latter is generally characterized by the *absence* of these peaks. In some cases, the vortex cores are even truly split into several smaller elements (Fig. 2(b)), totally separated by small zones showing the rise of coherence peaks. This has been verified by measuring the full spectra along lines through the vortex core, as in Fig. 2(a).

The smaller elements of a split vortex core cannot be related to separate vortices: first, the vortex-vortex repulsion makes it highly improbable that several vortex cores are so close to each other; second, counting all these elements as a flux quantum in Fig. 1(b), one finds a total flux through the surface that is far too large compared to the applied field. One should note here that the magnetic size of a flux line is of the order of the penetration depth λ , two orders of magnitude larger than the vortex core splitting observed here.

C. Vortex Motion

With subsequent spectroscopic images like Fig. 1(b), one can also study the vortex distribution as a function of time. We expect the vortex motion to be practically negligible, since we allowed the vortices to stabilize for more than 3 days²⁹. However, in Fig. 3 one can see that many vortices still have not reached totally stable positions. Many of them roughly stay on the same positions over the time span of our measurement, but others move to neighboring positions. Five different cases of moving vortices are indicated by the ellipses and the rectangle in Fig. 3.

In the panels on the left side the precise intensity of each point is difficult to read out directly. In order to investigate more quantitatively the time evolution of the vortex distribution, from one frame to the next, we show in the right part of Fig. 3 3D representations of the area that is marked by the rectangle in the 2D spectroscopic images. They give an idea of the gray scale used in the 2D images, and provide a detailed picture of the movement of the vortex core in front, from the right in Fig. 3(a) to the left in Fig. 3(c). The vortex core at the back does not move, and serves as a reference for the intensity. We remind that the intensity, or height in the 3D images, is a measure of the LDOS, which in a vortex core is different from the superconducting DOS. It is most interesting to see what happens in Fig. 3(b): the (moving) vortex core is *divided* between two positions. Thus, the vortex core moves from one position to the other, passing through an intermediate state where the vortex splits up between the two positions. Note that these two positions do not correspond to two vortices. In fact, the split vortex is characterized by the lower intensity compared to the nearby (reference) vortex. This means that the coherence peak at negative voltage does not completely

disappear, as it should if we had a complete and stable vortex at each of these positions. Note also that the density of vortices around the rectangular area on the left side in Fig. 3 will clearly be too high if we count the mentioned positions and all positions in the ellipses as individual flux quanta. The split vortex discussed here is not a unique example. Similar behaviour can be found for several other vortex cores, as indicated by the ellipses in Fig. 3. This gradual change of position is in striking contrast to the STS observations of moving vortices in NbSe₂^{30,31} and YBCO³².

D. Temperature Dependence

We performed measurements both at 4.2 and at 2.5 K, on samples cut from the same batch of crystals. The data taken at 2.5 K (see also Fig. 2) are fully consistent with the presented work at 4.2 K. In Fig. 4 we provide a general view of the vortex cores at 2.5 T, including an analogue of the moving vortex core of Fig. 3. Though it is hard to obtain any quantitative data, one can conclude that the vortex cores roughly have the same size, similar irregular shapes, and examples of split vortex cores can be easily found.

IV. DISCUSSION

A. Experimental Considerations

The observation of such a highly irregular pattern of vortex cores, as presented above, requires a careful analysis of the experimental setup. However, the fact that keeping exactly the same experimental conditions the number of vortex cores scales with the magnetic field, is a direct proof of the absence of artificial or noise-related structures in the spectroscopic images. Furthermore, since topographic images showed atomic resolution, there is no doubt that the spatial resolution of the STM is largely sufficient for the analysis of vortex core shapes.

The stability of the magnetic field can be verified by counting the number of vortices in the subsequent images at 6 T (Fig. 3). Since, excluding the split vortices marked by the ellipses, this number is constant (26 ± 3), we can exclude any substantial long time-scale variation of the magnetic field. Some variation in the total black area from one image to the other can be related to the tunneling conditions: a little more noise on the tunnel current will give a relatively large increase of the small zero-bias conductance. Since we divide by the zero-bias conductance to obtain the spectroscopic images, this may lead to some small variations in the integrated black area of the images.

B. Delocalization

Keeping in mind the randomness of the vortex distribution at 6 T due to pinning of vortices, we now relate both the split vortex cores (Fig. 2) and the intermediate state between two positions (Fig. 3 and Fig. 4) to the same phenomenon: the vortex cores appear to be delocalized between different positions which correspond to pinning potential wells, and during the measurement hop back and forth with a frequency that is too high to be resolved in this experiment. According to this analysis not only the distribution, but also the observed shape of the vortex cores is strongly influenced by pinning.

The pinning sites most probably result from inhomogeneities in the oxygen doping, which are thought to be responsible for the variations of the gap size (see experimental details). The distance over which the vortices are split corresponds to the average spacing between oxygen vacancies ($10 - 100 \text{ \AA}^{16}$). We did not observe any sign of resonant states related to impurities, as in recent STM experiments on BSCCO^{33,34}. The driving forces causing vortex movements in Fig. 3 and Fig. 4 are most probably due to a slow variation of the pinning potential, resulting from the overall rearrangement of vortices.

The vortex delocalization and movement presented here can directly be connected to the vortex creep as measured in macroscopic experiments, like magnetic relaxation¹³. The main difference, of course, is that we do not observe whole bundles of vortices moving over relatively large distances, but only *single* vortex cores that are displaced over distances much smaller than the penetration depth λ . That is, it will not be necessary to displace whole groups of vortices, many of which might be pinned much stronger than the delocalized vortices we observe. A second difference is the absence of a uniform direction of the movements in the STM images, most probably because the Lorentz driving forces have been reduced to an extremely small value (which also follows from the very gradual changes in Fig. 3 and Fig. 4).

C. Thermal Fluctuations versus Quantum Tunneling

Regarding now the mechanism responsible for the vortex delocalization, the main question is whether we are dealing with thermal fluctuations, or quantum tunneling between pinning potential wells. In fact magnetic relaxation measurements on BSCCO show a crossover temperature from thermal to quantum creep of $2 - 5 \text{ K}^{29,35-37}$, which means that with these STM measurements we are on the limit between the two.

In the case of thermally induced motion, there is a finite probability for the vortex to jump *over* the energy barrier between the two potential wells. The vortex is continuously moving from one site to the other, with a frequency that is too high to be resolved by our measurements. In the case of quantum tunneling, the vortex is

truly delocalized. That is, the vortex can tunnel *through* the barrier, and one observes a combination of two base states (i.e. positions), like in the quantum text book example of the ammonia molecule³⁸. Thermal fluctuations will lead to a continuous dissipative motion^{13,39} between the two sites; quantum tunneling gives a dissipationless state in which the vortex is *divided* between two positions.

An instantaneous observation of several base states of a quantum object would be impossible, since each measurement implies a collapse of the quantum wave function into one state. However, the STM gives only time averaged images, and with the tunneling current in this experiment we typically detect one electron per nanosecond. If the vortex core relaxes back to its delocalized state on a time scale smaller than nanoseconds, the vortex can appear delocalized in the STM images. Moreover, it should be clear that the long time (12 hours) between the subsequent images in Fig. 3 and 4 has nothing to do with the vortex tunneling time; it is tunneling of the vortex that allows the intermediate state. The creep of vortices (either by quantum tunneling or by thermal fluctuations) is a slow phenomenon here. At a given region the pinning potential due to inhomogeneities and interactions with other vortices evolves on a time scale of hours, shifting the energetically most favorable position from one site to the other. However, the tunneling occurs much faster ($< \text{ns}$) than this slow potential evolution, creating the possibility of a superposition of both states (positions), each with a probability depending on the local value of the pinning potential. Following the analogy of the ammonia molecule: a moving vortex core corresponds to an ammonia molecule submitted to an external external field ("overall pinning potential") that is slowly changing. Initially, due to this external field the state with the hydrogen atom at the left is more favorable, then the field changes such that left and right are equally stable ("split vortex"), and finally the right state is most probable: the hydrogen atom has moved from left to right on a long time scale, whereas the tunneling itself occurs on a much faster time scale. By the way, since the change of the local pinning potential results from a rearrangement of all surrounding vortices (over a distance $\sim \lambda$), the time scale of this change will still be strongly dependent on the (short) tunneling time itself.

In order to discuss the possibility of quantum tunneling, one should consider the tunneling time and the for our measurements negligible temperature dependence^{13,40}. The importance of the tunneling time is two-fold: the tunneling rate is strongly dependent on the time needed to pass through the pinning barriers (an effect which will be extremely difficult to measure directly); and in our measurements the tunneling time must be faster than the probe response time (as explained in the previous paragraph). From collective creep theory¹³ one can get an order-of-magnitude estimate for the tunneling time $t_c \sim \hbar/U(S_E/\hbar) \sim 10^{-11} \text{ s}$, with the Euclidian action for tunneling $S_E/\hbar \sim 10^2$ and the effective pinning energy $U \sim 10^2 \text{ K}$ derived from magnetic relaxation

measurements^{13,16,29,35–37}. This is clearly below the upper limit of 1 ns set by the probe response time.

For a discussion about the implications of the temperature independence of quantum tunneling, one should first consider the temperature dependence expected for vortex movements that result from thermal fluctuations. Thermally induced hopping between different pinning sites should be proportional to $\exp(U/k_B T)$, where U is again the effective pinning energy¹³. From magnetic relaxation measurements on BSCCO one can derive a value of about $10 - 10^3$ K for this quantity^{16,29,35–37}. Assuming for the moment that this U determines the hopping of individual vortices, it should then be compared to the Euclidian action for quantum tunneling, which with magnetic relaxation measurements is estimated to be $S_E/\hbar \sim 10^2$ ¹³, and plays a role like $U/k_B T$ in the Boltzman distribution. For measurements presented here, it is important to note again that they were taken more than 3 days after having increased the field from 0 to 6 T. Since for $B = 6$ T the induced current density j relaxes back to less than 0.01 of its initial value in about 10 seconds²⁹, we are clearly in the limit where j and thus the Lorentz driving forces (which reduce the energy barrier for vortex creep) approach zero. This means that the effective pinning potential U rises, if not to infinity like in isotropic materials, to a value which in principle is much higher than the one which determines vortex creep in magnetic relaxation measurements at comparable field strengths^{13,15}. With nearly zero Lorentz forces the tilt of the overall pinning potential will thus be small compared to the pinning barriers, making thermal hopping *over* the barriers highly improbable (at low temperatures). Quantum creep, in the limit of vanishing dissipation, is independent of the collective aspect of U , while the probability for thermal creep decreases as $\exp(-U/k_B T)$ ¹³. So one can expect quantum creep to become more important than thermal creep when more time has passed after having changed the field. In other words, in spite of the fact that the tilt of the overall pinning potential is small compared to the pinning barriers, the vortices can still move a little, i.e. disappearing and reappearing elsewhere.

However, the collective U may be higher than the pinning barriers for the individual vortex movements observed in our experiments. Thus, in order to find a lower bound for the latter, we also estimate U for the moving vortices from our microscopic measurement. First we calculate the magnetic energy of a vortex due to the interaction with its nearest neighbors, using

$$E_{int} = d \frac{\Phi_0^2}{8\pi^2 \lambda^2} \sum_i \left\{ \ln\left(\frac{\lambda}{r_i}\right) + 0.12 \right\}, \quad (1)$$

where d is the length of the vortex segment, Φ_0 is the flux quantum, λ the in-plane penetration depth and r_i the distance to its i th neighbor¹⁵. Parameters are conservatively chosen such to give a true minimum estimate for E_{int} (and thus for U): we restrict the out-of-plane extent of the vortices to zero and thus only take $d = 15$ Å,

the size of one double Cu-O layer⁴¹ ("pancake vortices"), and for λ take the upper bound of different measurements, 2500 Å^{42–44}. Taking the vortex in Fig. 3(b), and determining the positions between which it is divided as well as the positions of the neighboring vortices, one can find the difference between the magnetic interaction energies of the delocalized vortex at its two positions. We obtain $E_{int} \sim 120$ K. Now the absence of any vortex lattice indicates that the pinning potential wells are generally larger than the magnetic energy difference between the subsequent vortex positions, and Fig. 3(b) reflects a vortex state that is quite common in our measurements (Fig. 1). Following these arguments one can safely assume that the effective potential well pinning the vortex in Fig. 3 is larger than this difference: $U > E_{int} = 120$ K. in agreement with the estimates given above. So we obtain $U/k_B T > 10 - 10^2$ for temperatures around 4 K. In the limit of zero dissipation $S_E/\hbar \sim (k_F \xi)^2$. On the basis of STS experiments^{10,11} this can be estimated to be ≤ 10 . This value is smaller than the one quoted above, and suggests that quantum tunneling is dominant in our measurements.

The most direct evidence for quantum creep can be obtained from measurements at different temperatures. The hopping rate for thermally induced movements is given by $\omega_0 \exp(-U/k_B T)$, where U is the pinning potential, and ω_0 the characteristic frequency of thermal vortex vibration¹⁵. Assuming $U = 100$ K, and a conservatively large estimate of $\omega_0 \sim 10^{11} \text{ s}^{-1}$, the hopping rate should drop from 1 s^{-1} to 10^{-7} s^{-1} on cooling from 4.2 to 2.5 K. This gives a huge difference between the respective measurements at these temperatures. However, spectroscopic images at 4.2 and 2.5 K show the same pattern of moving and delocalized vortices. Following the same kind of estimations as above, the delocalized vortex at 2.5 K (Fig. 4) gave $U > 210$ K, which makes thermal creep even more unlikely here. Even if the frequency of the individual thermal vortex movements were too high to be resolved by our measurements *both* at 4.2 and at 2.5 K (this would mean a rather unrealistic characteristic frequency $\omega_0 > 10^{15}$), one would still expect to see a difference. As a matter of fact, the driving force for the vortex movements results from an overall rearrangement of vortices. This means that the displacements of vortices will always depend on the hopping frequency, and that even for very high hopping rates one should observe a reduction of the number of vortices that are displaced in our images, when the hopping rate is reduced by a factor 10^7 .

V. CONCLUSION

We observed vortex cores that were delocalized over several pinning potential wells. Regardless of the exact mechanism (thermal hopping or quantum tunneling) responsible for this delocalization, our measurements point

out that pinning effects not only dominate the distribution of the vortex cores, but also their shape. As a consequence intrinsic (four-fold?) symmetries of the vortex cores will be obscured in microscopic measurements. The delocalization of the vortex cores implies that the vortex cores in this study appear larger than their actual — unperturbed — size, indicating a coherence length that is even smaller than was expected on the base of previous studies¹¹.

The analysis given above strongly favors an interpretation in terms of quantum tunneling of vortex cores. This would not only mean the first microscopic signature of the vortex quantum tunneling as derived from magnetic relaxation measurements, it is also a further indication⁴⁵ that objects of larger size and complexity than one or several atoms can appear as a superposition of different quantum states.

ACKNOWLEDGMENTS

This work was supported by the Swiss National Science Foundation.

* E-mail: Bart.Hoogenboom@physics.unige.ch.

† Present address: University of California at San Diego, Department of Physics, 9500 Gilman dr., La Jolla CA 92093, USA.

- ¹ S.K. Yip and J.A. Sauls, Phys. Rev. Lett. **69**, 2264 (1992).
- ² G.E. Volovik, JETP Lett. **58**, 1174 (1993).
- ³ A.J. Berlinsky, A.L. Fletter, M. Franz, C. Kallin, and P.I. Soininen, Phys. Rev. Lett. **75**, 2200 (1995).
- ⁴ M.I. Salkola, A.V. Balatsky, and D.J. Scalapino, Phys. Rev. Lett. **77**, 1841 (1996).
- ⁵ M. Franz and Z. Tešanović, Phys. Rev. Lett. **80**, 4763 (1998).
- ⁶ K.A. Moler, D.J. Baar, J.S. Urbach, R. Liang, W.N. Hardy, and A. Kapitulnik, Phys. Rev. Lett. **73**, 2744 (1994).
- ⁷ A. Maeda, Y. Lino, T. Hanaguri, N. Motohira, K. Kishio, and T. Fukase, Phys. Rev. Lett. **74**, 1202 (1995).
- ⁸ B. Revaz, J.-Y. Genoud, A. Junod, K. Neumaier, A. Erb, and E. Walker, Phys. Rev. Lett. **80**, 3364 (1998).
- ⁹ M.H.S. Amin, I. Affleck, and M. Franz, Phys. Rev. B **58**, 5848 (1998).
- ¹⁰ I. Maggio-Aprile, Ch. Renner, A. Erb, E. Walker, and Ø. Fischer, Phys. Rev. Lett. **75**, 2754 (1995).
- ¹¹ Ch. Renner, B. Revaz, K. Kadowaki, I. Maggio-Aprile, and Ø. Fischer, Phys. Rev. Lett. **80**, 3606 (1998).
- ¹² S.H. Pan, E.W. Hudson, K.M. Lang, H. Eisaki, S. Uchida, and J.C. Davis, Nature **403**, 746 (2000).
- ¹³ G. Blatter, M.V. Feigel'man, V.B. Geschkenbein, A.I. Larkin, and V.M. Vinokur, Rev. Mod. Phys. **66**, 1125 (1994), and references therein.
- ¹⁴ M. Tinkham, Helv. Phys. Acta **61**, 443 (1988).

- ¹⁵ M. Tinkham, *Introduction to Superconductivity*, 2nd. ed. (McGraw-Hill, New York, 1996).
- ¹⁶ T.W. Li, A.A. Menovsky, J.J.M. Franse, and P.H. Kes, Physica C **257**, 179 (1996).
- ¹⁷ A. Erb, A.A. Manuel, M. Dhalle, F. Marti, J.-Y. Genoud, B. Revaz, A. Junod, D. Vasumathi, S. Ishibashi, A. Shukla, E. Walker, Ø. Fischer, R. Flükiger, R. Pozzi, M. Mali, and D. Brinkmann, Solid State Comm. **112**, 245 (1999).
- ¹⁸ R. Cubitt, E.M. Morgan, G. Yang, S.L. Lee, D.Mck. Paul, H.A. Mook, M. Yethiraj, P.H. Kes, T.W. Li, A.A. Menovsky, Z. Tarnawski, and K. Mortensen, Nature **365**, 407 (1993).
- ¹⁹ C. Caroli, P.G. de Gennes, and J. Matricon, Phys. Lett. **9**, 307 (1964).
- ²⁰ H.F. Hess, R.B. Robinson, R.C. Dynes, J.M. Valles, and J.V. Waszczak, Phys. Rev. Lett. **62**, 214 (1989).
- ²¹ Ch. Renner, A.D. Kent, Ph. Niedermann, Ø. Fischer, and F. Lévy, Phys. Rev. Lett. **67**, 1650 (1991).
- ²² B.W. Hoogenboom, M. Kugler, Ch. Renner, B. Revaz, I. Maggio-Aprile, and Ø. Fischer, Physica C (2000).
- ²³ S.H. Pan, E.W. Hudson, A.J. Gupta, K.-W. Ng, and J.C. Davis, preprint.
- ²⁴ Ch. Renner, Ph. Niedermann, A.D. Kent, and Ø. Fischer, J. Vac. Sci. Technol. A **8**, 330 (1990).
- ²⁵ A.D. Kent, Ch. Renner, Ph. Niedermann, J.-G. Bosch, and Ø. Fischer, Ultramicroscopy **42-44**, 1632 (1992).
- ²⁶ M. Kugler, Ch. Renner, V. Mikheev, G. Batey, and Ø. Fischer, Rev. Sci. Instrum. **71**, 1475 (2000).
- ²⁷ Ch. Renner, B. Revaz, J.-Y. Genoud, K. Kadowaki, and Ø. Fischer, Phys. Rev. Lett. **80**, 149 (1998).
- ²⁸ Ch. Renner and Ø. Fischer, Phys. Rev. B **51**, 9208 (1995).
- ²⁹ A.J.J. van Dalen, R. Griessen, and M.R. Koblischka, Physica C **257**, 271 (1996).
- ³⁰ Ch. Renner, Ph.D. thesis, University of Geneva, 1993.
- ³¹ A.M. Troyanovski, J. Aarts, and P.H. Kes, Nature **399**, 665 (1999).
- ³² I. Maggio-Aprile, Ch. Renner, A. Erb, E. Walker, and Ø. Fischer, Nature **390**, 487 (1997).
- ³³ A. Yazdani, C.M. Howald, C.P. Lutz, A. Kapitulnik, and D.M. Eigler, Phys. Rev. Lett. **83**, 176 (1999).
- ³⁴ E.W. Hudson, S.H. Pan, A.K. Gupta, K.-W. Ng., and J.C. Davis, Science **285**, 88 (1999).
- ³⁵ D. Prost, L. Fruchter, and I.A. Campbell, Phys. Rev. B **47**, 3457 (1993).
- ³⁶ K. Aupke, T. Teruzzi, P. Visani, A. Amann, A.C. Mota, and V.N. Zavaritsky, Physica C **209**, 255 (1993).
- ³⁷ D. Monier and L. Fruchter, Phys. Rev. B **58**, 8917 (1998).
- ³⁸ R.P. Feynman, R.B. Leighton, and M. Sands, *Lectures on Physics* (Addison-Wesley, Reading, Massachusetts, 1965), Vol. III.
- ³⁹ J. Bardeen and M.J. Stephen, Phys. Rev. **140**, A1197 (1965).
- ⁴⁰ G. Blatter and V.B. Geschkenbein, Phys. Rev. B **47**, 2725 (1993).
- ⁴¹ D.R. Harshman and Jr. A.P. Mills, Phys. Rev. B **45**, 10684 (1992), and references therein.
- ⁴² Ref. 41 gives $\lambda = 2500 \text{ \AA}$, but for a sample that has not been O₂ annealed. In Ref. 44 it is shown that this indeed results in a higher λ . Since the samples discussed here are over-doped (O₂ annealed), one can safely adopt the values for

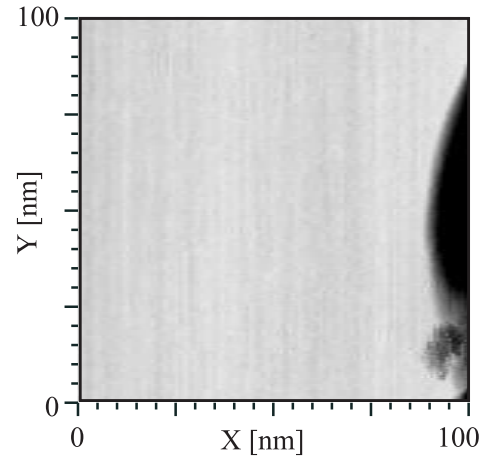
optimum doped or overdoped samples, considerably lower than 2500 \AA ^{43,44}.

⁴³ J.C. Martínez, S.H. Brongersma, A. Koshelev, B. Ivlev, P.H. Kes, R.P. Griessen, D.G. de Groot, Z. Tarnavski, and A.A. Menovsky, Phys. Rev. Lett. **69**, 2276 (1992).

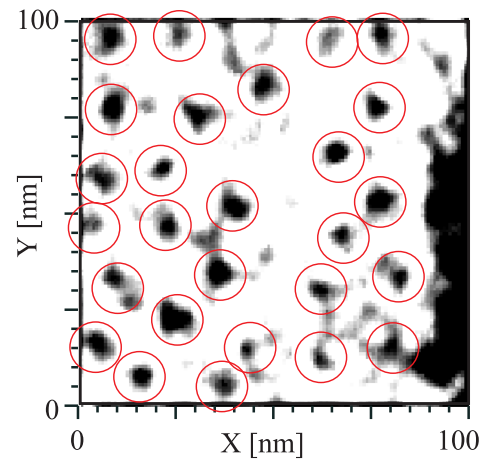
⁴⁴ O. Waldmann, F. Steinmeyer, P. Müller, J.J. Neumeier, F.X. Régi, H. Savary, and J. Schneck, Phys. Rev. B **53**, 11825 (1996).

⁴⁵ M. Arndt, O. Nairz, J. Vos-Andreae, C. Keller, G. van der Zouw, and A. Zeilinger, Nature **401**, 680 (1999).

(a) Topographic image



(b) $B = 6 \text{ T} \sim 26 \Phi_0 / 27 \times$ 



(c) $B = 2 \text{ T} \sim 7 \Phi_0 / 7 \times$ 

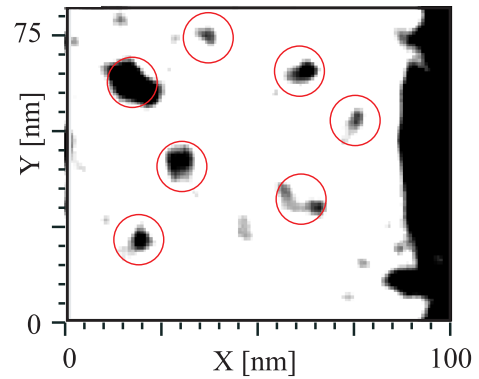


FIG. 1. (a) $100 \times 100 \text{ nm}^2$ topographic image of the BSCCO surface at 4.2 K and 6 T, taken at high bias voltage, $V_{bias} = 0.4 \text{ V}$, $I_t = 0.6 \text{ nA}$. The structure at the right gradually increases in height from 0 nm (lightest gray) to almost 5 nm (fully black at the right border), and is thus much larger than any atomic details. The surface roughness of the gray part is about 1 \AA . (b) Spectroscopic image of the same area, taken simultaneously with (a); dark spots correspond to vortex cores, the dark region at the right corresponds to the degraded surface of the structure already observed in (a). For the surface excluding this topographic structure one should expect 26 vortices, the image contains 27 (the circles around the vortex cores serve as a guide to the eye). (c) Part of the same region, at 2 T, image taken after all measurements at 6 T. The number of vortices in the image again perfectly corresponds to what one should expect for the given surface.

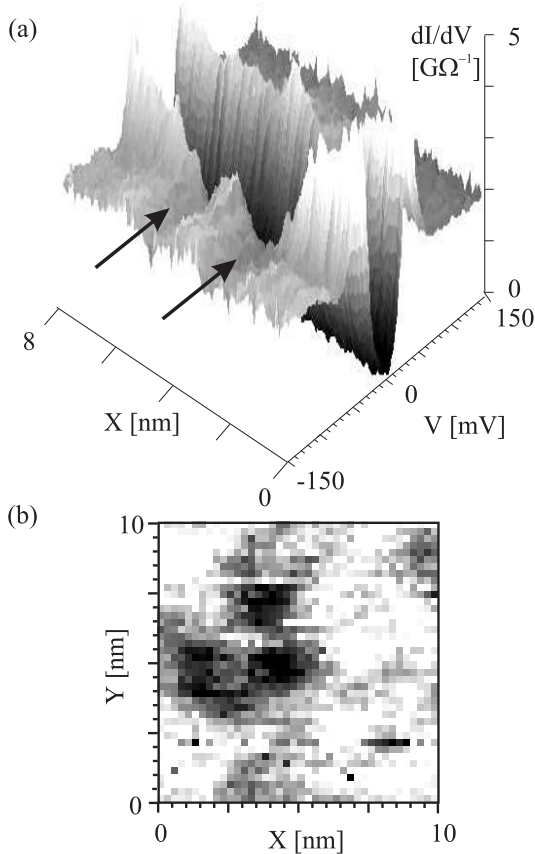


FIG. 2. (a) Spectra along a trace through a vortex core ($B = 6 \text{ T}$, $T = 2.5 \text{ K}$) reveal that in between regions with vortex core-like spectra (indicated by the two arrows) the superconducting coherence peaks come up again. (b) Image of a vortex core consisting of several separate elements. ($B = 6 \text{ T}$, $T = 4.2 \text{ K}$).

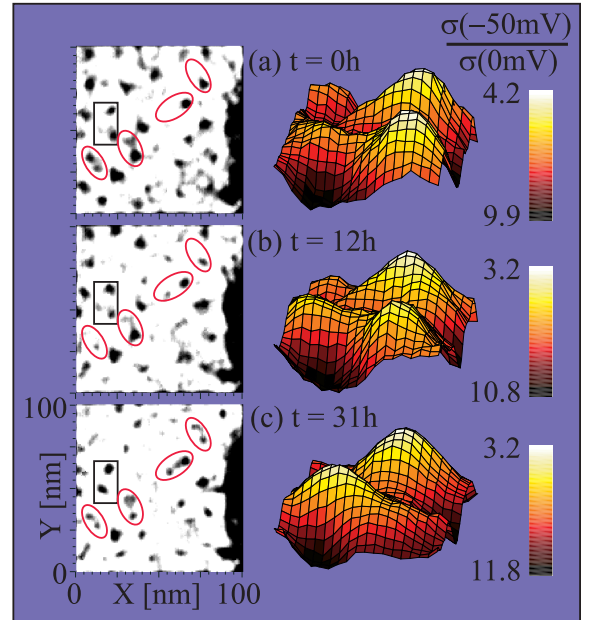


FIG. 3. Sequence of images (each taking about 12 hours) to study the behaviour of the vortex cores in time, $B = 6 \text{ T}$, $T = 4.2 \text{ K}$. t corresponds to the starting time of each image. (a) $t = 0$; (b) $t = 12\text{h}$; (c) $t = 31\text{h}$. Left: 2D representation. Right: 3D images of the zone marked by the rectangles in the 2D images. The vortex core seems to be split in (b), before it totally moves from one position in (a) to the other in (c).

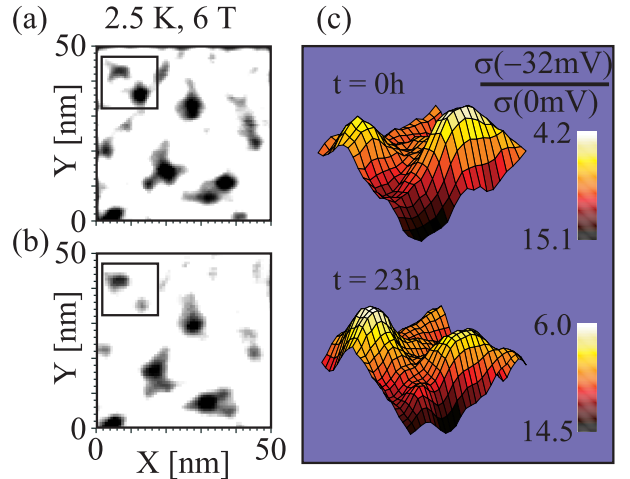


FIG. 4. Subsequent images ((a) and (b)) at $B = 6 \text{ T}$, $T = 2.5 \text{ K}$. In (c) a 3D representation of the square marked in (a) and (b). At 2.5 K one observes the same phenomena as at 4.2 K in Fig. 2 and Fig. 3.